

Compton Profile and Electron Distribution of Iron

Walter C. Phillips*

Physics Department, Brandeis University, Waltham, Massachusetts 02154

and

R. J. Weiss

Army Materials and Mechanics Research Center, Watertown, Massachusetts 02172

(Received 8 May 1972)

The Compton profile for bcc single-crystal iron has been measured using Mo and Ag $K\alpha$ x rays. The observed profile is somewhat narrower than that calculated for a free-atom Fe $3d^8$ configuration. Within the experimental uncertainty of $\pm 3\%$, the profiles measured with the x-ray scattering vector along the [111] and [100] crystal directions show no anisotropy. Using the doubly and triply degenerate $3d$ -orbital description, a simple model is proposed which is consistent with the results of the Compton (momentum-density), charge-density, and unpaired-spin-density measurements.

I. INTRODUCTION

The iron Compton-profile measurements were undertaken primarily to determine the band-electron momentum distribution. A secondary purpose was to evaluate the usefulness of the technique for obtaining accurate momentum-density information when comparatively low-energy radiation (~ 20 keV) is used with elements of atomic number ~ 25 . Compton scattering from polycrystalline Fe has been measured with 17-keV $MoK\alpha$ radiation in a preliminary experiment by Cooper and Williams,¹ and at 60 keV using a Ge-Li detector by Felsteiner, Fox, and Kahane.²

Other experimental determinations of band-electron distributions in Fe with which the Compton results can be compared are the momentum distribution measured by positron annihilation,³ the unpaired spin density measured by neutron diffraction,⁴ and the charge density measured by x-ray diffraction.^{5,6} Comparison of the measured Compton profile with profiles derived from calculated wave functions can provide a fairly stringent test of the calculations.

II. EXPERIMENT

The apparatus was similar to that described elsewhere, but employed a more stable data-acquisition system with more precise $\theta/(2\theta)$ tracking.⁷ The housing enclosing the x-ray tube and Fe sample was evacuated in order to remove air from the beam path. Air between the Mo target and sample contributed 42% of the Compton scattering at the Compton peak when the housing was not evacuated. Both $MoK\alpha$ (17.5 keV) and $AgK\alpha$ (22.2 keV) radiation was used. For the Mo and Ag experiments, the spectrographic x-ray tubes were operated at 60 keV, 40 mA and 80 keV, 30 mA, respectively; Soller-slit collimators on the tubes limited the angle

between extreme rays striking the sample to $\pm 3^\circ$ and $\pm 6^\circ$, respectively, and the mean Compton scattering angle $2\theta_c = 158^\circ$ and 159° , respectively. In each experiment the energy analysis of the scattered beam was made with a LiF crystal using the (400) reflection and a pair of Soller slits. The total instrumental resolution (full width at half-maximum) due to divergences allowed by the Soller collimators and the mosaic spread of the analyzing crystal was 0.31 and 0.42 a.u., respectively, for Mo and Ag. The peak counting rates were 145 and 180 counts/min, and the Compton/background intensity = 2.9 and 1.8 at the peak for Mo and Ag, respectively.

Four bcc Fe samples were used: (i) an Fe polycrystalline powder, (ii) a strain-annealed Fe crystal, (iii) a 1.5-at.% Si α -stabilized crystal, and (iv) a 1.5-at.% Al α -stabilized crystal. For both Mo and Ag experiments, data were obtained with the x-ray-scattering vector approximately along the [100] crystal direction [crystals (ii) and (iii)], and with the scattering vector approximately along the [111] direction [crystal (iv)]. No impurity lines were observed from any sample, nor was there any significant difference between profiles measured with different crystals for the same incident wavelength.

Considerable care was necessary in orienting the crystal sample in order to minimize Bragg scattering of the continuum radiation in the wavelength region of the Compton peak. Thus, e.g., in the "[111] orientation" the crystal was actually oriented with the scattering vector 4° from the [111]. Even with the crystal set to exclude most Bragg scattering from the data, some elastic scattering will be present because of the density of reciprocal lattice points and the long Bragg-peak tails resulting primarily from thermal diffuse scattering (TDS), i.e., phonons. This additional scattering is not important in our experiment, be-

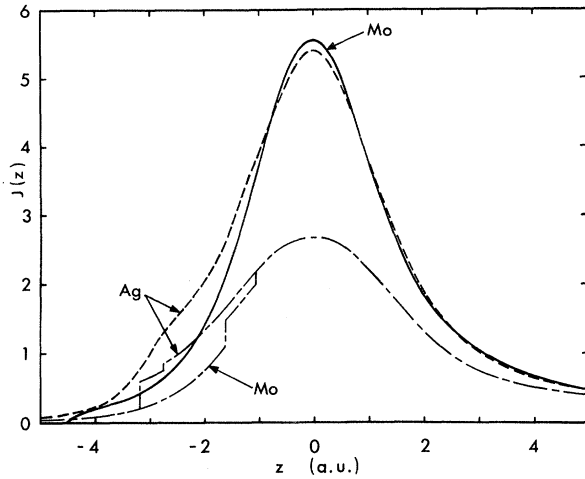


FIG. 1. Normalized Compton profiles for Fe measured with $\text{MoK}\alpha$ radiation (average of [100] and [111] data) and $\text{AgK}\alpha$ radiation ([111] data). Each curve represents the sum of hundreds of scans at 0.06-a.u. intervals with a total of 40 000 x rays counted per interval at the peak. The calculated $2s^2 2p^6 3s^2 3p^6$ impulse-approximation core profiles are also shown. Since $\text{AgK}\alpha$ radiation produces a larger energy shift than $\text{MoK}\alpha$, the $2s$ and $2p$ Compton thresholds are shifted further from the peak for Ag. While only data for $z > 0$ are presented in the final experimental results, the small differences between the Ag and Mo results in Table I may in part be due to the influence of the $2s$ - $2p$ levels.

cause its magnitude is small compared to other experimental uncertainties.

III. DATA ANALYSIS

The theory of Compton scattering has been described in recent articles and will not be treated here.^{8,9} When the electron binding energy E_B is small compared to the energy transferred to the electron in the Compton collision (the impulse approximation), the Compton profile $J(z)$ and the one-electron ground-state momentum wave function $\chi_i(\vec{p})$ are related by the expression

$$J(z) = \frac{1}{2} \sum_i \int_{|\vec{z}|}^{\infty} |\chi_i(\vec{p})|^2 dp_x dp_y, \quad (1)$$

where the scattering vector \vec{s} is perpendicular to the x - y plane,

$$\chi_i(\vec{p}) = (2\pi)^{-3/2} \int_0^{\infty} \psi_i(\vec{r}) e^{-i\vec{p}\cdot\vec{r}} d^3r, \quad (2)$$

$$z = \frac{mc}{2\lambda_0 \sin\theta_c} \left(\Delta\lambda - \frac{2h}{mc} \sin^2\theta_c \right) \times \left[1 + \Delta\lambda + \left(\frac{\Delta\lambda}{2\lambda_0 \sin\theta_c} \right)^2 \right]^{-1/2}, \quad (3)$$

λ_0 is the wavelength of the incident x ray, λ is the wavelength of the scattered x ray, and $\Delta\lambda = \lambda - \lambda_0$. The energy transferred to the scattered electron at the center of the Compton peak is 1090 and 1720 eV in the Mo and Ag experiments, respectively. Thus

the Fe $1s$ electrons do not contribute to the Compton scattering. The $3s$, $3p$, and $3d$ electrons satisfy the impulse-approximation condition [Eq. (1)], whereas the $2s$ and $2p$ electrons do not ($E_B \approx 850$ and 710 eV, respectively). The normalized Compton profiles presented in Fig. 1 illustrate the differences between the data collected with $\text{MoK}\alpha$ and $\text{AgK}\alpha$ radiation. The calculated impulse-approximation $2s^2 2p^6 3s^2 3p^6$ cores for both wavelengths are also shown in Fig. 1. Below E_B the $2s$ and $2p$ electrons do not contribute to Compton scattering, and for energy transfers not much greater than E_B , departures from the impulse approximation are expected.⁸ No calculation has been done which properly treats scattering in this regime. Thus values of $J(z)$ for $z < 0$, where the uncertainty in the core calculation is greatest, are not included in the results reported below. For $z \geq 0$, the experimental $J(z)$ curves obtained at the two wavelengths agree to within the experimental uncertainty of $\pm 3\%$.

In order to obtain the experimental $J(z)$ curve the data (x-ray counts vs $\text{LiF } 2\theta$) are analyzed in the following way. A smooth visual curve is drawn through the data. The background from Compton and TDS scattering of the bremsstrahlung continuum is approximated by a straight line. The slope and height of the background line are adjusted by trial and error until the resulting $J(z)$ agrees with the value calculated for a Hartree-Fock Fe $2s^2 2p^6 3s^2 3p^6 3d^8$ configuration (the band electrons contribute very little at $z=5$), and the difference between the background and the data below the $K\alpha$ threshold equals the $K\beta$ Compton scattering. (The $K\beta$ Compton profile was measured in a preliminary experiment.) Requiring the experimental profile to match the calculated profile at $z=5$ a.u. essentially eliminates background uncertainties from significantly influencing the resulting normalized experimental profile for $z > 0$. With this linear background subtracted, the data are corrected for the wavelength dependence of the Compton cross section, the absorption in the sample, and the reflectivity of the LiF. The $K\alpha_1$ and $K\alpha_2$ components of the Compton scattering are separated using the Rachinger method, and the resulting curves are converted to an electron-momentum (z) scale and the area normalized such that $\int_0^{5.00} J(z) dz = 10.37$, the calculated impulse-approximation area for $2s^2 2p^6 3s^2 3p^6 3d^8$ electrons. This normalization is obviously only a first approximation (better for the Ag than the Mo experiment), because it assumes that the $2s^2 2p^6$ area for $z > 0$ is correctly given by the impulse approximation. Some discussion of this point can be found in Ref. 9; the experimental justification is the agreement between the results of the Mo and Ag experiments within the experimental uncertainty.

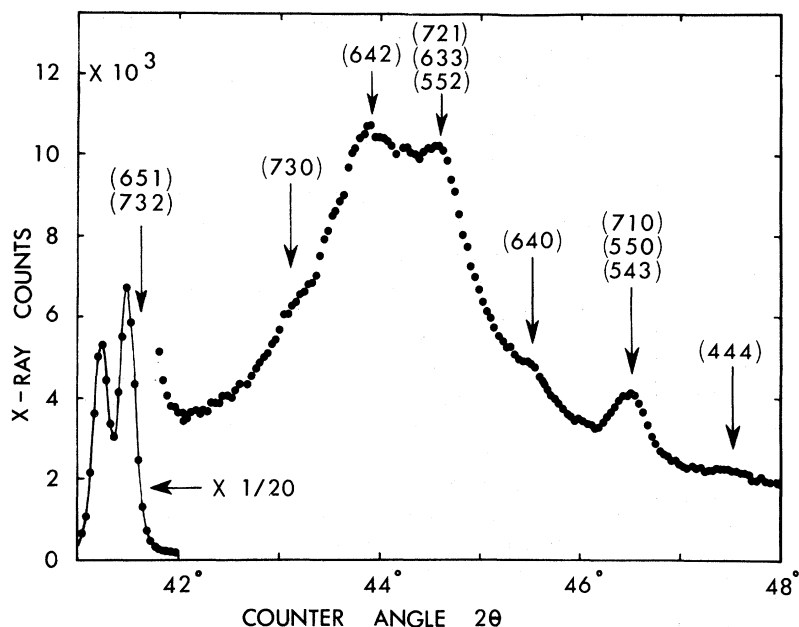


FIG. 2. $\text{MoK}\alpha$ radiation scattered from polycrystalline Fe at $2\theta_c = 158^\circ$. Superimposed on the Compton profile are the Bragg peaks due to elastic scattering of the bremsstrahlung. Bragg scattering can be eliminated by using single-crystal samples. The $\text{MoK}\alpha_2$ peak is enhanced relative to the $\text{K}\alpha_1$ TDS peak because of elastic scattering from the tails of the (651), (732) Bragg reflections.

IV. RESULTS

Initially an Fe polycrystalline (compressed powder) sample was used, as we were mainly interested in measuring the over-all shape of the Compton profile rather than searching for possible anisotropies. Previous Compton experiments on low- Z (< 20) elements have routinely employed polycrystalline samples. However, it became evident after data were accumulated for several days that Bragg scattering of continuum radiation was contributing significantly to the measured intensity. The result of a 5-day polycrystalline experiment with $\text{MoK}\alpha$ is shown in Fig. 2. Bragg peaks with high multiplicity are contributing $> 10\%$ of the maximum Compton intensity. (The width of the Bragg peaks $\approx 0.1|\Delta\theta_c|$ under the conditions employed in our experiments.) Clearly meaningful results can not be extracted from data obtained using polycrystalline samples of high- Z ($Z \sim 25$) materials with simple unit cells for wavelengths $\sim 0.5 < \lambda < 1.0 \text{ \AA}$, because there will always be Bragg peaks in the wavelength range spanned by the Compton profile.¹⁰ As λ decreases, the ratio of Compton/elastic scattering will become greater, and for λ short enough polycrystalline samples of high- Z materials can be used.

At both Mo and Ag wavelengths, profiles were measured for each of the three crystals described above. The average of the sum of these results, representing 120 000 x rays counted per 0.06 a. u. interval at the peak, is shown in Fig. 3 and given in Table I. The uncertainty in the final $J(z)$ arising from counting statistics is much smaller than the

$\sim \pm 2\%$ uncertainty at $J(0)$ due to background subtraction and wavelength corrections.

The experimental band-electron profile, i. e., the difference between the average experimental $J(z)$ and the impulse-approximation core of Fig. 3, is shown in Fig. 4 and Table I. Assuming the validity of the calculated core, the error in the band profile due to all experimental uncertainties

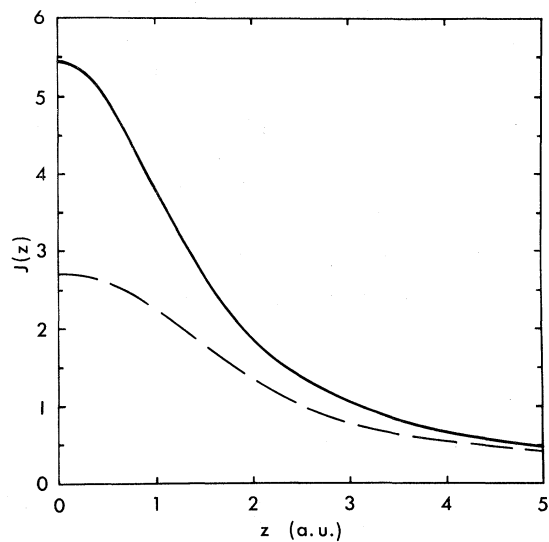


FIG. 3. Experimental Fe Compton profile, representing the average of all data at both Mo and Ag wavelengths, with 120 000 x rays counted per 0.06-a. u. interval at the peak. The calculated $2s^2 2p^6 3s^2 3p^6$ impulse-approximation-core profile is shown by the dashed curve.

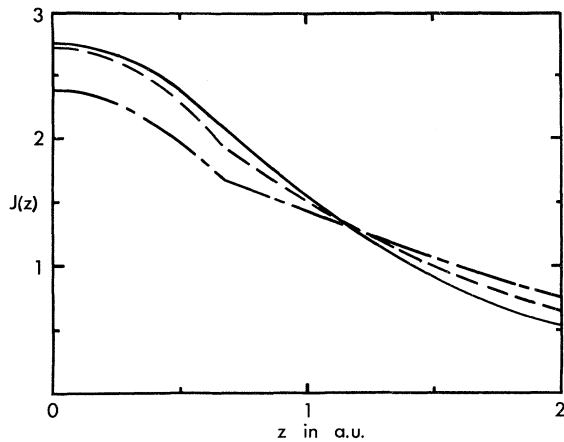


FIG. 4. Experimental Fe band-electron profile (solid curve). The calculated profiles are for the spherically averaged Mn $3d^{7.2}+0.8$ free-electron (dashed curve) and Fe $3d^{7.2}+0.8$ free-electron (dot-dashed curve) configurations discussed in the text.

is $\pm 4\%$ at $J(0)$.

Momentum-density anisotropy was examined at both wavelengths by comparing profiles measured

for [100] and [111] crystal orientations. No difference in the profiles measured at a given wavelength was detected outside of the experimental uncertainty of each measurement of $\pm 3\%$, i. e., the measured difference

$$2[J_{111}(0) - J_{100}(0)]/[J_{111}(0) + J_{100}(0)] < 3\%.$$

Considering the effects of core subtraction and $\alpha_1\alpha_2$ deconvolution, this implies a band-electron profile anisotropy of $\leq 5\%$ for these two directions at $z=0$.

V. ANALYSIS OF RESULTS

A. X-Ray Results

The analysis of the following x-ray data was undertaken to see whether a consistent and reasonable set of wave functions could account for these experimental results on iron: (a) the Compton profile, (b) the absolute x-ray-scattering factors,⁵ (c) intensity differences between the (411)-(330) and (600)-(442) paired x-ray reflections,⁶ and (d) the small anisotropy in the Compton profile.

We assumed a band-electron configuration $3d^{7.2}+0.8$ free electrons, and attempted to fit the above data to within the quoted experimental errors.

TABLE I. Measured and calculated Compton profiles for Fe.

z	Experimental $J(z)$		$2s^2 2p^6 3s^2 3p^6$ Impulse app. $J(z)$	Experimental band $J(z)$	Band $J(z)$ for Mn $3d^7$ -Cr $3d^6$ model	
	Mo	Ag			[100]	[111]
0.0	5.54	5.33 \pm 0.16	2.69	2.75 \pm 0.11	2.65	2.88
0.2	5.46	5.28	2.68	2.69	2.60	2.79
0.4	5.21	5.11	2.63	2.53	2.46	2.55
0.6	4.79	4.70	2.54	2.21	2.04	2.13
0.8	4.30	4.25	2.41	1.87	1.82	1.78
1.0	3.79	3.79 \pm 0.11	2.25	1.54 \pm 0.08	1.55	1.50
1.2	3.32	3.34	2.07	1.26	1.32	1.26
1.4	2.88	2.94	1.89	1.02	1.11	1.06
1.6	2.47	2.55	1.69	0.82	0.92	0.88
1.8	2.12	2.20	1.51	0.65		
2.0	1.84	1.91 \pm 0.06	1.34	0.53 \pm 0.04	0.64	0.61
2.2	1.61	1.67	1.18	0.46		
2.4	1.44	1.49	1.05	0.41		
2.6	1.29	1.32	0.94	0.36		
2.8	1.16	1.18	0.85	0.32		
3.0	1.03	1.05 \pm 0.05	0.77	0.27 \pm 0.04	0.27	0.26
3.2	0.94	0.94	0.69	0.25		
3.4	0.85	0.84	0.64	0.20		
3.6	0.77	0.76	0.60	0.16		
3.8	0.71	0.69	0.57	0.13		
4.0	0.66	0.64 \pm 0.05	0.53	0.12 \pm 0.04	0.10	0.10
4.2	0.61	0.60	0.50	0.10		
4.4	0.57	0.57	0.47	0.10		
4.6	0.53	0.55	0.44	0.10		
4.8	0.50	0.53	0.42	0.09		
5.0	0.46	0.51 \pm 0.04	0.41	0.07 \pm 0.03	0.05	0.05

Using the doubly and triply degenerate $3d$ -orbital description, we had at our disposal the ratio of t_{2g} to e_g $3d$ electrons (the total of course was held fixed at 7.2) and the radial $3d$ functions for the t_{2g} and e_g orbitals. By trial and error it was possible to account for the experimental results employing the following parameters: 5.0 ± 0.1 t_{2g} -symmetry electrons having a Mn Hartree-Fock (HF) radial wave function (for a $3d^7$ configuration), 2.2 ± 0.1 e_g -symmetry electrons having a Cr HF radial wave function (for a $3d^6$ configuration).¹¹ In terms of the e_g - t_{2g} orbital description, the scattering factor f and the Compton profile $J(z)$ per electron in a cubic crystal are given by

$$\begin{aligned} f_t(hkl) &= \langle j_0 \rangle_t - \frac{1}{3} A \langle j_4 \rangle_t, \\ f_e(hkl) &= \langle j_0 \rangle_e + \frac{1}{2} A \langle j_4 \rangle_e, \\ \langle j_n \rangle &= \int_0^\infty R^2 j_n(sr) r^2 dr, \\ A &= \frac{3(h^4 + k^4 + l^4) - 9(h^2 k^2 + h^2 l^2 + k^2 l^2)}{(h^2 + k^2 + l^2)^2}, \end{aligned} \quad (4)$$

where j_n is the spherical Bessel function, s the magnitude of the x-ray-scattering vector, R the radial part of the $3d$ wave function, and t_{2g} and e_g are abbreviated by t and e .

$$\begin{aligned} J(z)_t &= \frac{5}{2\pi} \int_{|z|}^\infty [j_{\frac{3}{2}}^*(pr)]_t^2 \left[\alpha_t + \beta_t \left(\frac{z}{p}\right)^2 + \delta_t \left(\frac{z}{p}\right)^4 \right] p dp, \\ j_{\frac{3}{2}}^*(pr)_t &= \int_0^\infty R_t j_{\frac{3}{2}}(pr) r^2 dr, \end{aligned} \quad (5)$$

and a corresponding expression for the e_g . α , β , and δ are coefficients that depend on the direction of the x-ray-scattering vector relative to the crystal direction.¹² The functions $\langle j_0 \rangle$ and $\langle j_4 \rangle$ have been evaluated by Watson and Freeman¹³ for various $3d^n$ free-atom configurations and the functions

$$\int [j_{\frac{3}{2}}^*(pr)]^2 (z/p)^n p dp, \quad n=0, 2, 4 \quad (6)$$

have been evaluated by Weiss¹⁴ for the same $3d$ wave functions. To obtain the total scattering factor and Compton profile per atom the core and free-

electron contributions must be added to the $3d$ contributions. For the core-electrons free-atom HF functions for Fe were employed,^{13,15} while the $4s$ contribution was assumed to be free-electron-like with a correction for correlation. For free electrons the contribution to the Bragg peaks is zero and the contribution to the Compton profile is

$$J(z) = \frac{3}{4p_F} \left[1 - \left(\frac{z}{p_F} \right)^2 \right] \text{ per electron,} \quad (7)$$

where p_F is the Fermi momentum. For 0.8 electron per atom in Fe, $p_F = 0.67$. To allow for correlation the free-electron profile was scaled to the difference between the observed lithium valence-electron profile¹⁶ and the profile obtained from Eq. (7). [The correlation correction reduces the calculated $J(0)$ by only 3%.]

The results of the calculations employing the orbital populations and radial wave functions cited above are given in Table I and Table II, together with two band calculations for the scattering factors.^{17,18} The agreement with experiment is quite good using these functions, better than either band calculation for the elastic-scattering data.

As an example of the sensitivity of the results to the choice of parameters, using a single radial function, the best fit is obtained for the Mn $3d$ function and e_g - t_{2g} population 2.2 and 5.0, which gives $f[110] = 18.09$, $J_{100}(0) = 5.24$, $J_{111}(0) = 5.53$, and $f^2(442)/f^2(600) = 1.042$. The Compton profile is shown in Fig. 4. The only significant change from the model above is a small increase in the discrepancy with the measured $f[110]$. Replacement of the Cr and Mn $3d$ radial functions by V and Fe $3d$ radial functions for the e_g and t_{2g} orbitals, respectively, gives $f[110] = 18.10$, $J_{100}(0) = 5.37$, $J_{111}(0) = 5.49$, and $f^2(442)/f^2(600) = 1.082$. Thus the agreement between the measured and calculated $f[110]$ and $f^2(442)/f^2(600)$ becomes somewhat poorer. Keeping the Cr and Mn $3d$ radial functions but changing the e_g - t_{2g} population to 2.6 and 4.6 yields $f[110] = 17.94$,

TABLE II. Measured and calculated scattering factors for Fe. The calculations are for the Mn $3d^7$ -Cr $3d^6$ model discussed in the text and for the band calculations cited.

hkl	$(\sin\theta)\lambda$	Fe core	$2.2f_{e_g}$	$5.0f_{t_{2g}}$	f_{total}	Measured (Ref. 5)	Band calculations (Ref. 18) (Ref. 17)		$3d^7 4s$ free atom	
110	0.247	15.15	0.74	2.08	17.97	17.6 ± 0.2	18.37	18.55	18.7	
200	0.349	13.14	0.62	0.82	14.58	14.7 ± 0.2	15.12	14.89	15.3	
220	0.494	10.62	0.07	0.52	11.21	11.1 ± 0.2	11.53	11.65	11.6	
330	0.741	7.97	-0.06	0.11	8.02	7.7 ± 0.2	8.08	8.03	8.1	
411	0.741	7.97	0.10	-0.16	7.91	7.7 ± 0.2	8.05	8.02	8.1	
442	1.048	6.38	0.08	-0.09	6.37					
600	1.048	6.38	0.13	-0.30	6.20					
					$f^2(330)/f^2(411)$	1.028	1.023 ± 0.005	1.007	1.002	
					$f^2(442)/f^2(600)$	1.054	1.05 ± 0.01	1.012	*	

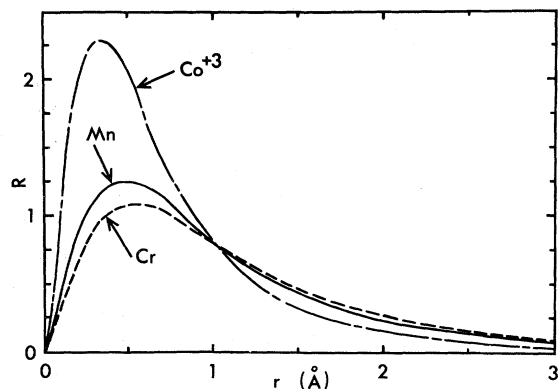


FIG. 5. Hartree-Fock radial wave functions (Ref. 11) for Cr $3d^6$ (dashed curve) and Mn $3d^7$ (solid curve) used in calculating an Fe Compton profile in agreement with the measurements. The Co^{+3} function (dot-dashed curve) gives a calculated unpaired-spin-radial form factor in agreement with experiment.

$J_{100}(0) = 5.45$, $J_{111}(0) = 5.51$, and $f^2(442)/f^2(600) = 1.02$. Again, agreement with the measured $f^2(442)/f^2(600)$ is poorer.

While the final choice of parameters is not unique, the calculations are sufficiently representative to provide a qualitative picture of the electron distribution.

The Compton profile calculated for 7.2 electrons in an Fe $3d^7$ free-atom configuration + 0.8 free electrons is also shown in Fig. 4. The fit to the measured profile is poor, and the calculated scattering factors (given in Table II) are in poor agreement with the observations. A better fit to the profile at $J(0)$ is obtained using an Fe $3d^6$ + 2 free-electron configuration, but again the agreement between the calculated and observed scattering factors is poor.

B. Neutron Results

If the same radial functions employed above are now used to calculate the magnetic-scattering factors, they are in serious error with experiment. The neutron-diffraction measurements of Shull and Yamada,⁴ which measured the unpaired spin density in Fe, can be accounted for using the Co^{+3} $3d^6$ or Fe $3d^8$ free-atom radial wave function and an orbital e_g/t_{2g} population ratio = 1.13. The Co^{+3} radial function is considerably contracted relative to the radial functions used above to evaluate the charge and momentum density. Figure 5 shows the Cr, Mn, and Co^{+3} wave functions. Thus the present analysis supports the expectation that the unpaired spin arises primarily from electrons near the top of the band with $3d$ free-atom-like radial wave functions which are contracted relative to the total $3d$ wave function.

C. Positron Results

In order to compare our x-ray results with the results of positron-annihilation measurements, it is necessary to take into account the positron wave function. If we assume that the annihilated electron was unperturbed by the positron before annihilation, then the only conceptual difference between the x-ray and positron measurements is to replace $\psi_i(\vec{r})$ in Eq. (2) by the product $\psi_i(\vec{r})\psi_p(\vec{r})$, where $\psi_p(\vec{r})$ is the ground-state Bloch wave function for the positron. Figure 6 shows a comparison between the Compton band profile and the positron band profile, i. e., the Fe single-crystal results of Mijnaerends³ with a calculated core (~20% of the total annihilation radiation) subtracted.¹⁹ (The positron profile has been normalized to the Compton area.) If we assume the positron wave function is essentially constant in the band-electron overlap region, both profiles should be identical. An inspection of Fig. 6 shows that this is not the case.

Mijnaerends³ has calculated the positron curve by evaluating the positron wave function in the Wakoh-Yamashita potential¹⁷ used in the band calculations^{17,18} cited in Table II. With this positron wave function and the band wave function from the Wakoh-Yamashita potential,¹⁹ Mijnaerends has calculated the positron curve¹⁹ shown in Fig. 6, which is still not in good agreement with the positron results. However, it is interesting that here again the experimental results depart from the calculation in the same direction as the x-ray results, i. e., an expansion of the charge density in

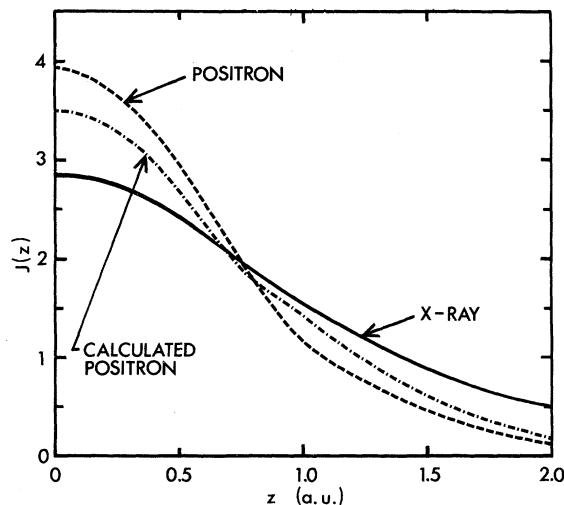


FIG. 6. Experimental Fe band-electron Compton profile (solid curve), experimental positron-band profile (Refs. 3 and 19) normalized to the same area for $0 < z < 2$ a. u. (dashed curve), and the positron profile calculated by Mijnaerends (Refs. 3 and 19) using the Wakoh-Yamashita potential (dot-dashed curve).

the solid, hence a narrowing of the momentum density.

VI. CONCLUSIONS

We have found a reasonable set of HF free-atom $3d^{7.2}$ and 0.8 free-electron wave functions which predict a Compton profile and x-ray form factor in agreement with the measured results. The band calculations cited appear to be at significant variance with the elastic-scattering and positron measurements, notably the band results are too Fe-free-atom-like. Perhaps a fresh examination of the band calculations would be useful.

Wakoh and Yamashita¹⁷ construct their potential function from the free-atom $3d$ functions of Watson,²⁰ with minor modifications for crystalline effects. It is perhaps not surprising that the charge density they obtain using this potential is very free-atom-like. There is of course no *a priori* justification for this procedure. Perhaps a more accurate potential could be obtained from *ab initio* calculation of the Fe molecule (a central atom and eight nearest neighbors arranged as in the bcc lattice). The potential around the central atom of the Fe molecule could then be used for the band calculations. It would also be instructive to use the potential obtained from the measured x-ray-scattering factors. Self-consistency in a band calculation based on an assumed starting potential does not necessarily provide sufficient justification for its accuracy. A wide variety of starting potentials may lead to a wide variety of "self-consistent"

charge densities.

At present the largest uncertainty in the band-electron-momentum distributions obtained from low-energy Compton-scattering measurements in $3d$ metals is introduced by the $2s^2 2p^6$ core subtraction. An accurate theoretical treatment of Compton scattering from electrons with binding energies of the order of the electron recoil energy is not available. Thus there is no rigorous method for separating the $2s^2 2p^6$ core-electron contribution from the observed profile. The error in the band-electron profile resulting from the subtraction of an impulse-approximation core may be greater than the uncertainties introduced by counting statistics or other experimental errors and correction. The experimental justification for using the impulse core is the agreement between the profiles measured with Mo and Ag radiation. This agreement, together with the fact that the largest core contribution in the band-electron region comes from the $3s^2 3p^6$ electrons, certainly suggests that the Compton results are sufficiently accurate at present to provide a test of band calculations, particularly when used in conjunction with elastic-x-ray-scattering, neutron-diffraction, and positron annihilation results.

ACKNOWLEDGMENTS

We wish to thank Professor C. G. Shull and Professor S. Berko for their help and advice, and Dr. P. E. Mijnarends for making his results available prior to publication.

*Research supported by National Science Foundation Grant No. GU-3852.

¹M. Cooper and B. G. Williams, *Phil. Mag.* **17**, 1079 (1968).

²J. Felsteiner, R. Fox, and S. Kahane, *Solid State Commun.* **9**, 457 (1971).

³P. E. Mijnarends (private communication); *Physica* (to be published).

⁴C. G. Shull and Y. Yamada, *J. Phys. Soc. Japan* **17**, Supp. B-III, i (1962); C. G. Shull, *Electronic Structure and Alloy Chemistry of the Transition Elements* (Interscience, New York, 1963), p. 69.

⁵B. W. Batterman, D. R. Chipman, and J. J. DeMarco, *Phys. Rev.* **122**, 68 (1961).

⁶J. J. DeMarco and R. J. Weiss, *Phys. Letters* **18**, 92 (1965).

⁷W. C. Phillips and R. J. Weiss, *Phys. Rev.* **171**, 790 (1968).

⁸P. Eisenberger and P. M. Platzman, *Phys. Rev. A* **2**, 415 (1970).

⁹R. Currat, P. D. DeCicco, and R. J. Weiss, *Phys. Rev. B* **4**, 4256 (1971).

¹⁰Because of Bragg scattering, the error in the preliminary results in Ref. 1 is probably greater than the

author's reported error.

¹¹R. E. Watson, Technical Report No. 12, S. S. M. T. G., M. I. T., 1959 (unpublished). These Hartree-Fock (HF) radial functions are chosen simply for convenience, since their scattering factors and Compton profiles are already tabulated (see Refs. 13 and 15).

¹²R. J. Weiss, *Phil. Mag.* **14**, 403 (1966).

¹³R. E. Watson and A. J. Freeman, *Acta Cryst.* **14**, 27 (1961).

¹⁴R. J. Weiss, *X-Ray Determination of Electron Distributions* (North-Holland, Amsterdam, 1966), p. 185.

¹⁵R. J. Weiss, A. Harvey, and W. C. Phillips, *Phil. Mag.* **17**, 241 (1968).

¹⁶W. C. Phillips and R. J. Weiss, *Phys. Rev. B* **5**, 755 (1972).

¹⁷S. Wakoh and J. Yamashita, *J. Phys. Soc. Japan* **21**, 1712 (1966).

¹⁸P. D. DeCicco and A. Kitz, *Phys. Rev.* **162**, 486 (1967).

¹⁹The positron profile was obtained by integrating the weighted average of the [100], [110], and [111] momentum densities in Ref. 3.

²⁰R. E. Watson, *Phys. Rev.* **119**, 1934 (1960).